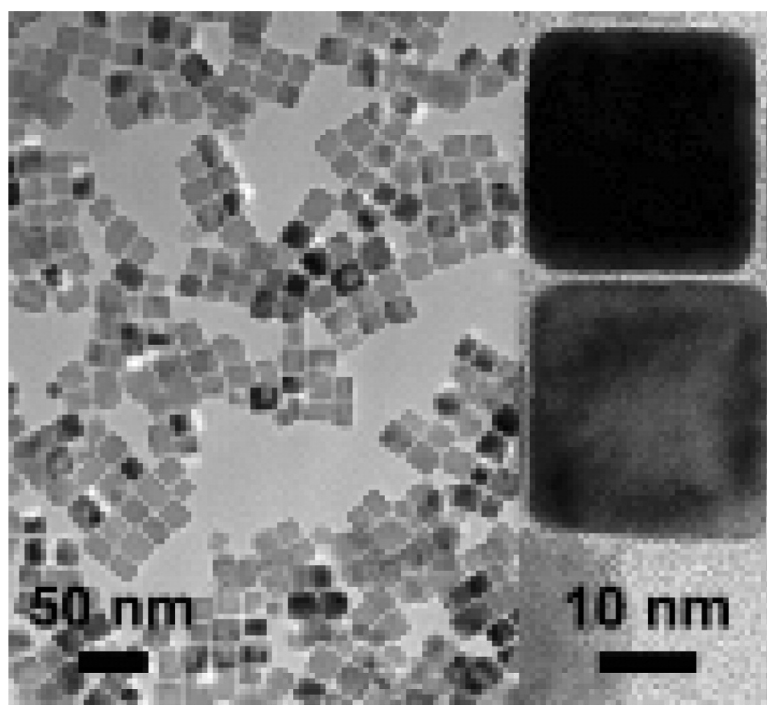


Surfactant-Controlled Size and Shape Evolution of Magnetic NanoparticlesGyu Leem, Subhasis Sarangi, Shishan Zhang, Irene Rusakova,
Audrius Brazdeikis, Dmitri Litvinov, and T. Randall Lee*Cryst. Growth Des.*, 2009, 9 (1), 32-34 • DOI: 10.1021/cg8009833 • Publication Date (Web): 02 December 2008Downloaded from <http://pubs.acs.org> on April 15, 2009**More About This Article**

Additional resources and features associated with this article are available within the HTML version:

- Supporting Information
- Access to high resolution figures
- Links to articles and content related to this article
- Copyright permission to reproduce figures and/or text from this article

[View the Full Text HTML](#)**ACS Publications**
High quality. High impact.

Surfactant-Controlled Size and Shape Evolution of Magnetic Nanoparticles

Gyu Leem,[†] Subhasis Sarangi,[‡] Shishan Zhang,[†] Irene Rusakova,[‡] Audrius Brazdeikis,[‡] Dmitri Litvinov,[§] and T. Randall Lee^{*,†}

Departments of Chemistry and Chemical Engineering, Texas Center for Superconductivity and Department of Physics, and Center for Nanomagnetic Systems, University of Houston, 4800 Calhoun Road, Houston, Texas 77204-5003

Received September 3, 2008

ABSTRACT: This manuscript describes a simple one-pot reaction that affords cuboid iron–manganese oxide nanoparticles with unprecedented dimensions as large as 33 ± 5 nm (average body-centered diagonal) in monodisperse form. Our unique synthetic method, which requires no multiple growth steps typical of other methods, utilizes the thermal decomposition of metal precursor complexes in the presence of specifically tailored surfactants and/or mixtures of surfactants. The size and shape of these unusually large magnetic nanoparticles (MNPs) can be manipulated at will simply by adjusting the surfactant composition, leading to enhanced control over the dimensions of the nanoparticles because of the surface-differentiating influence of the functional end groups. Our surfactant system utilizes two types of surface ligands: one strongly bound to the metal surface and the others loosely bound. This combination of ligands plays an important role in controlling particle size and morphology. With an eye toward potential biomedical applications, the magnetic properties of the MNPs were investigated through their $M-H$ hysteresis loop behavior at 290 K. More importantly, when exposed to a magnetic field, relaxation measurements of these MNPs afforded Néel relaxation times of 3.4 s at an average body-centered diagonal size of 29 ± 4 nm.

Monodisperse magnetic nanoparticles with controlled sizes and shapes are of great interest for fundamental science and for both existing and developing technological applications. The morphology of MNPs strongly influences their chemical and physical properties, and especially their magnetic and electrical properties. More specifically, the requirements for most biomedical applications strongly depend on the size, shape, functionality, and magnetization of the MNPs. For example, the superparamagnetic nature and narrow size distribution about a particular value are essential for magnetically driven hyperthermia,¹ nanoparticle-based imaging,² cell-receptor actuation,³ and relaxation immunoassays,⁴ whereas in magnetic resonance imaging (MRI), the crystalline symmetry, size of the magnetic core, and nature of the surface coating determine the T1, T2, and T2* relaxivities of these particles.⁵ Furthermore, when administered intravenously, the corporal distribution and subsequent rate of elimination are largely determined by particle size, where small superparamagnetic nanoparticles less than ~ 30 nm in diameter are known to exhibit a longer plasma half-life than do larger particles (e.g., up to ~ 100 nm).⁶

Despite this important advantage of small nanoparticles, many applications, including magnetic cell separation, remote cell control, magnetofection, and magnetic drug delivery, require large MNPs (ca. 200–500 nm) because the magnetic force exerted on a MNP is proportional to its magnetic moment and particle volume (larger particles = greater force). In fact, better contrast is observed in MRI when using large vs small magnetic nanoparticles.⁷ Moreover, the control of size distribution of MNPs is one of the most crucial parameters for biomedical applications.¹ The combination of narrow size distribution and appropriate particle size is required not only for magnetic fluids,⁸ but also magnetic labels in magnetoresistive biosensors and biochips.⁹

The relationship between the shape and the magnetic properties of MNPs is another important factor because MNPs with different shape can influence the crystal orientation in an assembly,¹⁰ and specifically contoured MNPs exhibit net shape anisotropy.¹¹ A

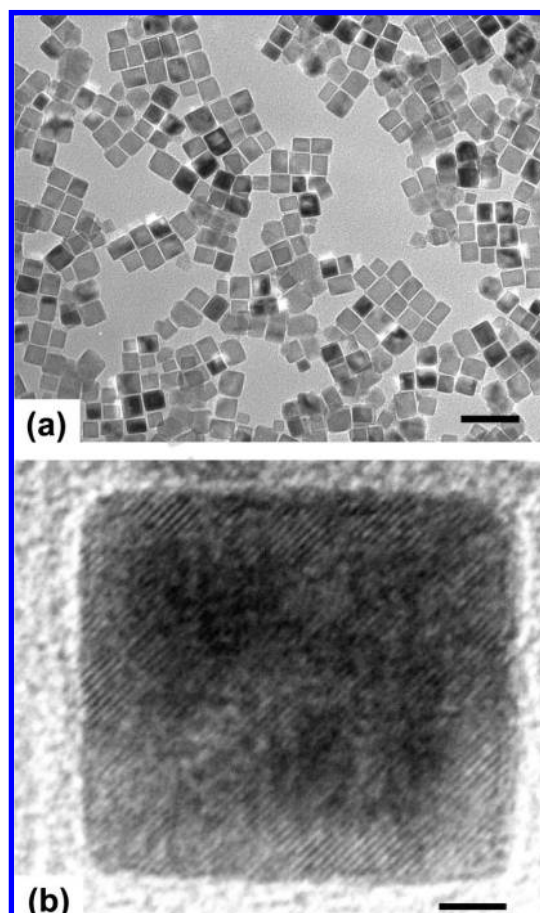


Figure 1. (a) Conventional bright-field (scale bar = 50 nm) and (b) HR-TEM image (scale bar = 2 nm) TEM images. The average body-centered diagonal size shown here is 29 ± 4 nm. Two analogous preparations afforded identical distributions of 33 ± 5 nm.

shape-controlled assembly, which can lead to an aligned magnetic easy axis,¹⁰ is highly attractive for a variety of emerging nanotechnological applications, including biosensing, bioimaging, and

* To whom correspondence should be addressed. Tel: (713) 743-2724. Fax: (281) 754-4445. E-mail: trlee@uh.edu.

[†] Departments of Chemistry and Chemical Engineering, University of Houston.

[‡] Texas Center for Superconductivity and Department of Physics, University of Houston.

[§] Center for Nanomagnetic Systems, University of Houston.

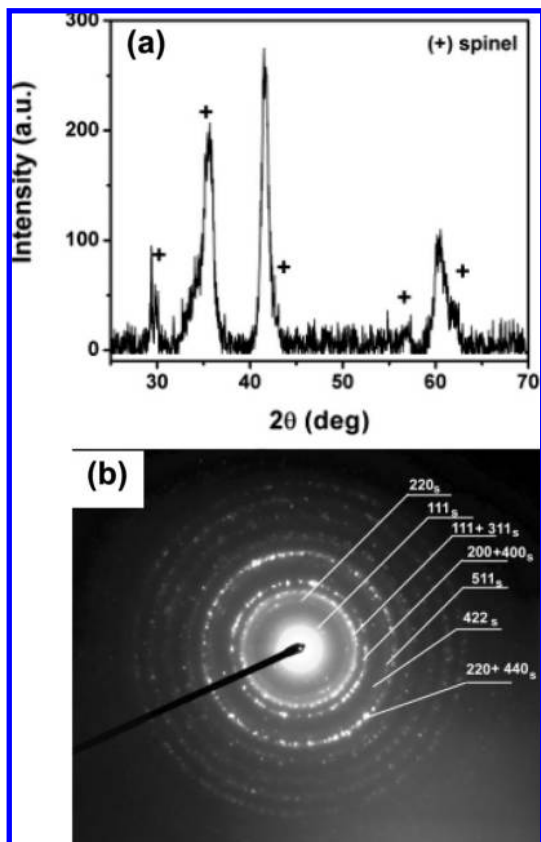


Figure 2. (a) XRD and (b) TEM-SAED patterns of polycrystalline iron–manganese oxide samples. Rings with s subscripts arise from the spinel MnFe_2O_4 phase, and the other rings arise from $\text{Fe}_{1-x}\text{Mn}_x\text{O}$ ($0 < x < 1$) phases.

therapeutics. Consequently, there is an urgent need for a simple, fast, reliable, and inexpensive route to a versatile class of monodisperse MNPs that are suitable for this diverse array of applications.

One of most useful magnetic oxide nanoparticles, iron–manganese oxide, has been prepared using a variety of methods, such as reverse micelle microemulsion,¹² mechanical ball milling,¹³ thermal decomposition,^{9,14,15} and coprecipitation.¹⁶ However, certain applications, including tumor ablation,^{8,17} magnetic imaging,^{2,5} and nanomagnetic cellular manipulation,¹⁸ require iron–manganese oxide nanoparticles that are larger than those currently available in monodisperse form (i.e., ≥ 20 nm in diameter). Until now, no reliable synthetic route for the preparation of such particles has been reported.

The decomposition product from a 1:1 mixture of $\text{Fe}(\text{acac})_3$ and $\text{Mn}(\text{acac})_2$ was analyzed by transmission electron microscopy (TEM), X-ray diffraction (XRD), and dynamic light scattering (DLS). Specifically, conventional and high-resolution (HR) TEM imaging, selected area electron diffraction (SAED), and energy-dispersive X-ray spectroscopy (EDS) methods were used. The conventional TEM image in Figure 1a demonstrates that the morphology of the nanocrystals is uniformly cuboid; further, the HR TEM image in Figure 1b confirms that the particles are composed largely of single crystals. We note that the slightly blurry contrast for some of the nanocrystals in Figure 1a probably arises from the presence of minor defects.

Importantly, analysis by EDS confirms that only Mn and Fe were present in the samples. Furthermore, examination of the XRD and SAED patterns found that the face-centered cubic (fcc) $\text{Fe}_{1-x}\text{Mn}_x\text{O}$ phases ($0 < x < 1$, $Fm\bar{3}m$; No. 225) with a small amount of MnFe_2O_4 spinel phase ($Fd\bar{3}m$; No. 227, $a = 8.402$ Å) were the predominant species present (see Figure 2). There are two possible phases that possess the same symmetry (No. 225) and similar lattice parameters: $\text{Fe}_{0.664}\text{Mn}_{0.336}\text{O}$, $a = 4.36$ Å, and $\text{Fe}_{0.798}\text{Mn}_{0.202}\text{O}$, $a = 4.342$ Å. These phases cannot be distinguished in the XRD and

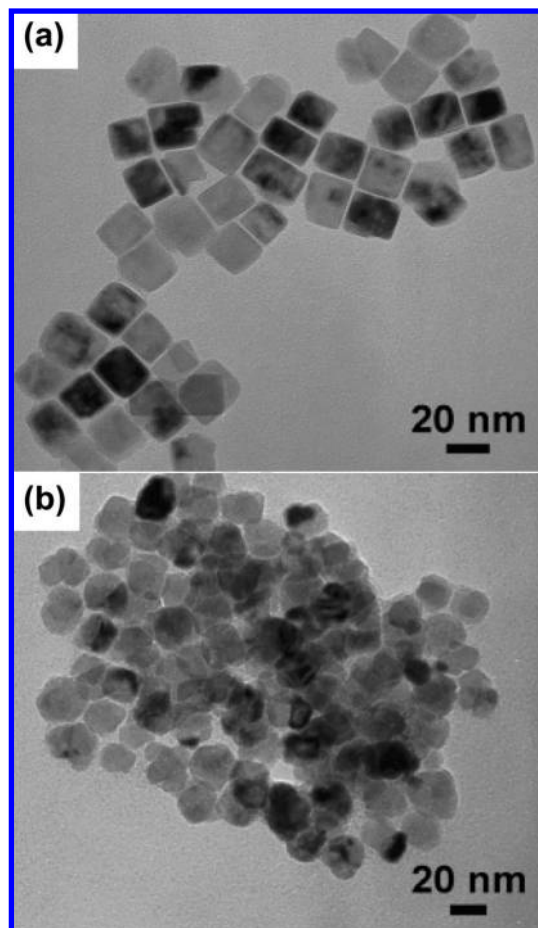


Figure 3. Shape variation of iron–manganese oxide nanoparticles upon variation of the ester content. Ratio of 16-heptadecenoic acid:ethyl heptadecenoate equals (a) 4:1 and (b) 1:1.

SAED patterns because of line broadening, which is known to be caused either by small nanoparticle size,¹⁹ the presence of two or more different phases, and/or a high density of crystal defects.

The growth rate has been shown to be an important factor in controlling the shape of magnetic nanoparticles.²⁰ Moreover, the wet chemical synthesis of monodisperse large nanoparticles typically involves precise control over the growth rate by using a high concentration of metal cation and controlling the strength of binding between various ligands and the emerging metal surface. In control experiments here, the use of analytically pure 16-heptadecenoic acid failed to afford large monodisperse nanoparticles (see the Supporting Information, Figure S1), giving instead an inhomogeneous mixture of particle shapes and sizes. Separately, a decrease in the $\text{Mn}(\text{acac})_2/\text{Fe}(\text{acac})_3$ ratio from 1:1 afforded iron–manganese oxide nanoparticles as irregular cuboids (see the Supporting Information, Figure S2).

Peng et al have reported an analogous observation regarding the morphology of CdSe nanocrystals prepared using crude (i.e., 90%) trioctylphosphine oxide (TOPO).²¹ The impurities (alkyl phosphonic and phosphinic acids) in technical grade TOPO are strongly bound to the cadmium ions, leading to the synthesis of rod-like CdSe nanocrystals. Similarly, the behavior observed in our system can be rationalized on the basis of the differential binding of 16-heptadecenoic acid and the contaminant(s) to the growing metal surface in the presence of a 1:1 ratio of Mn and Fe reagents. As the ¹³C and ¹H NMR data confirm (see the Supporting Information, Figures S3 and S4), our crude surfactant is contaminated with ethyl heptadecenoate and trace amounts of ethanol. We propose that the carboxylic anions bind strongly and nonselectively to the nanoparticle surface during the nucleation and growth process,^{20,22} which leads to nonselective or isotropic growth. In contrast, the residual ester species bind less tightly but more selectively, which leads to

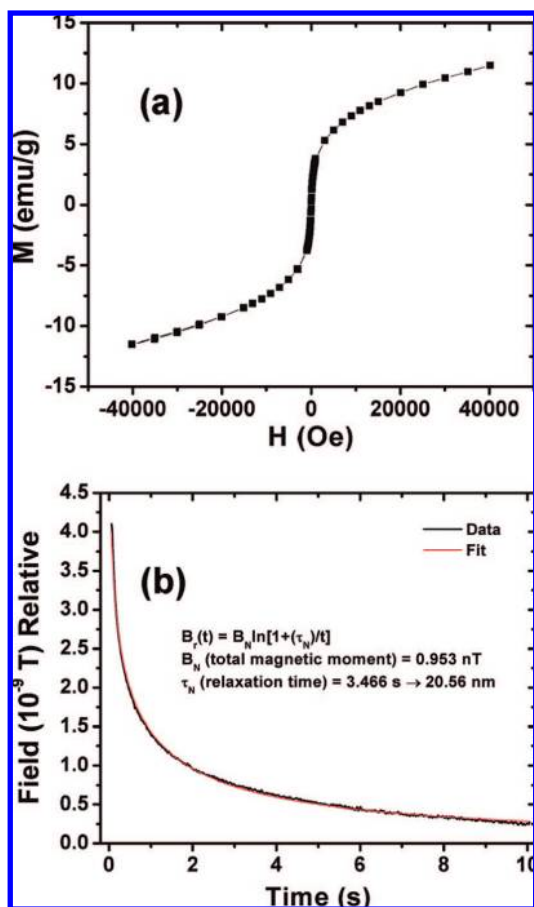


Figure 4. (a) Hysteresis loop of superparamagnetic iron–manganese oxide nanoparticles at room temperature and (b) magnetic relaxation curve of iron–manganese oxide nanoparticles magnetized at a field of 2 mT. The solid curve is the corresponding Néel relaxation fit.

anisotropic growth from a preferred crystalline face. Separate syntheses in which we added selected amounts of the ester contaminant to pure 16-heptadecenoic acid led to the formation of nanoparticles identical to those in Figure 1; moreover, increasing the amount of the ester from 10 to 50% led to increased aggregation and a greater distribution of nonuniform shapes for the product nanoparticles (see Figure 3). Similarly, a previous study found that the substitution of oleic acid with methyl oleate gives rise to highly polydisperse iron oxide nanoparticles.²³ Taken together, these studies collectively support our proposal that the ester contaminant associated with our crude 16-heptadecenoic acid is a key participant in the mechanism responsible for the growth of large monodisperse iron–manganese oxide nanoparticles. To examine further the processes occurring during the nucleation and growth stages, additional mechanistic studies are currently underway.

We also evaluated the key magnetic characteristics of our iron–manganese oxide nanoparticles. In particular, magnetic hysteresis loops and magnetic relaxation were measured for these particles at room temperature. The superparamagnetic nature of these particles is characterized by M – H hysteresis loop behavior at 290 K and rapid relaxation. The particles show superparamagnetic behavior, which is indicated by the vanishing coercivity in the hysteresis curve (Figure 4a) and the Néel relaxation time^{24,25} of 3.4 s from the relaxation curve (Figure 4b). The relaxation of the nanoparticles was measured after switching magnetic field off in the time window between 50 ms and 10 s. Néel relaxation in this time frame should occur for particles with diameters on the order of 20 nm, which is roughly consistent with the TEM data (average body-centered diagonal size of 29 ± 4 nm) and DLS data (hydrodynamic diameter of 32 nm). We note that monodisperse

particles of this size represent an ideal compromise for many biomedical applications,¹ offering the potential for both a strong magnetic moment⁷ and a long intravenous half-life.⁶

With the successful synthesis of these large magnetic oxide nanoparticles, we will explore their utility in a variety of applications. As noted above, the unprecedented dimensions of these magnetic nanoparticles in monodisperse form renders them attractive for use in various in vivo medical diagnostic and therapeutic applications, such as magnetic imaging^{2,5,7} and hyperthermia-based tumor ablation,^{8,17} respectively. Furthermore, control over the shape and size of MNPs can be used to influence the crystal orientation and packing geometry in ordered assemblies, which can be further utilized ex vivo in single-molecule biosensing applications.⁹

Acknowledgment. We thank the National Science Foundation (ECS-0404308), the Texas Center for Superconductivity, and the Robert A. Welch Foundation (Grant E-1320) for generous financial support of this work.

Supporting Information Available: Details regarding the preparation and characterization of the nanoparticles (PDF). This material is available free of charge via the Internet at <http://pubs.acs.org>.

References

- (1) Mornet, S.; Vasseur, S.; Grasset, F.; Duguet, E. *J. Mater. Chem.* **2004**, *14*, 2161.
- (2) Gleich, B.; Weizenecker, J. *Nature* **2005**, *435*, 1214.
- (3) Mannix, R. J.; Kumar, S.; Cassiola, F.; Montoya-Zavala, M.; Feinstein, E.; Prentiss, M.; Ingber, D. E. *Nat. Nanotechnol.* **2008**, *3*, 36.
- (4) Weitschies, W.; Kötz, R.; Bunte, T.; Trahms, L. *Pharm. Pharmacol. Lett.* **1997**, *7*, 1.
- (5) Tromsdorf, U. I.; Bigall, N. C.; Kaul, M. G.; Bruns, O. T.; Nikolic, M. S.; Mollwitz, B.; Sperling, R. A.; Reimer, R.; Hohenberg, H.; Parak, W. J.; Förster, S.; Beisiegel, U.; Adam, G.; Weller, H. *Nano Lett.* **2007**, *7*, 2422.
- (6) Neuberger, T.; Schöpf, B.; Hofmann, H.; Hofmann, M.; Rechenberg, B. v. *J. Magn. Magn. Mater.* **2005**, *293*, 483.
- (7) Lee, J.-H.; Huh, Y.-M.; Jun, Y.-W.; Seo, J.-W.; Jang, J.-T.; Song, H.-T.; Kim, S.; Cho, E.-J.; Yoon, H.-G.; Suh, J.-S.; Cheon, J. *Nat. Med.* **2007**, *13*, 95.
- (8) Gijs, M. A. M. *Microfluid. Nanofluid.* **2004**, *1*, 22.
- (9) Graham, D. L.; Ferreira, H. A.; Freitas, P. P. *Trends Biotechnol.* **2004**, *22*, 455.
- (10) Zeng, H.; Rice, P. M.; Wang, S. X.; Sun, S. *J. Am. Chem. Soc.* **2004**, *126*, 11458.
- (11) Hyeon, T. *Chem. Commun.* **2003**, 927.
- (12) Vestal, C. R.; Zhang, Z. *Nano Lett.* **2003**, *3*, 1739.
- (13) Muroi, M.; Street, R.; McCormick, P. G.; Amighian, J. *Phys. Rev. B* **2001**, *63*, 184414.
- (14) Song, Q.; Ding, Y.; Wang, Z. L.; Zhang, Z. J. *Chem. Mater.* **2007**, *19*, 4633.
- (15) Balaji, G.; Gajbhiye, N. S.; Wilde, G.; Weissmüller, J. *J. Magn. Magn. Mater.* **2002**, *242–245*, 617.
- (16) Ghosh, M.; Lawes, G.; Gayen, A.; Subbanna, G. N.; Reiff, W. M.; Subramanian, M. A.; Ramirez, A. P.; Zhang, J.-P.; Seshadri, R. *Chem. Mater.* **2004**, *16*, 118.
- (17) Daou, T. J.; Pourroy, G.; Begin-Colin, S.; Grenèche, J. M.; Ulhaq-Bouillet, C.; Legare, P.; Bernhardt, P.; Leuvrey, C.; Rogez, G. *Chem. Mater.* **2006**, *18*, 4399.
- (18) Dobson, J. *Gene Ther.* **2006**, *13*, 283.
- (19) Bronstein, L. M.; Huang, X.; Retrum, J.; Schmucker, A.; Pink, M.; Stein, B. D.; Dragnea, B. *Chem. Mater.* **2007**, *19*, 3624.
- (20) Burda, C.; Chen, X.; Narayanan, R.; El-Sayed, M. A. *Chem. Rev.* **2005**, *105*, 1025.
- (21) Peng, X.; Manna, L.; Yang, W.; Wickham, J.; Scher, E.; Kadavanich, A.; Alivisatos, A. P. *Nature* **2000**, *404*, 59.
- (22) Wu, N.; Fu, L.; Su, M.; Aslam, M.; Wong, K. C.; Dravid, V. P. *Nano Lett.* **2004**, *4*, 383.
- (23) Willis, A. L.; Turro, N. J.; O'Brien, S. *Chem. Mater.* **2005**, *17*, 5970.
- (24) Néel, L. *Ann. Geophys.* **1949**, *5*, 99.
- (25) Brown, W. F., Jr. *Phys. Rev.* **1963**, *130*, 1677.